

# Effect of diamino((2-((2-aminoethyl)amino)ethyl)amino)methanethiol on the Corrosion Resistance of Carbon Steel in Simulated Concrete Pore Solutions

Tao Ji<sup>1, 2</sup>, Fubin Ma<sup>3</sup>, Dalin Liu<sup>4</sup>, Xiaoying Zhang<sup>3</sup>, Xiong Zhang<sup>1</sup>, Qi Luo<sup>1, 5, \*</sup>

<sup>1</sup> School of Materials Science and Engineering, Tongji University, Shanghai, 201804, China

<sup>2</sup> China Construction Eighth Engineering Division Co. Ltd, Shanghai 200135, China

<sup>3</sup> Institute of Oceanology, Chinese Academy of Sciences, Qingdao, 266071, China

<sup>4</sup> School of Civil Engineering and Architecture, Nanchang University, Nanchang, 330031, China

<sup>5</sup> School of Materials Science and Engineering, Nanchang University, Nanchang, 330031, China

\*E-mail: [luoqi@ncu.edu.cn](mailto:luoqi@ncu.edu.cn)

Received: 9 March 2018 / Accepted: 10 April 2018 / Published: 10 May 2018

---

Diamino((2-((2-aminoethyl)amino)ethyl)amino)methanethiol was synthesized, and its inhibition performance on carbon steel in simulated concrete pore solutions was studied by means of electrochemical techniques, scanning electron microscopy and quantum chemical calculation. The results showed that the inhibiting performance of this inhibitor was excellent, and the obtained inhibition efficiencies from different experiments were in good agreement from different experiments. Polarization curves revealed that the inhibitor acted as a mixed-type inhibitor, suppressing the anodic and cathodic corrosion reaction processes of carbon steel by forming a protective film on its surface. Electrochemical impedance spectroscopy measurements revealed that the charge transfer process in the corrosion reaction was retarded because of the protection film formed on the surface of the carbon steel. The absorption mechanism of the inhibitor molecules on the carbon steel surface was analysed using a quantum chemical study.

---

**Keywords:** corrosion inhibitor; carbon steel; electrochemical techniques; simulated concrete pore solutions; chloride

## 1. INTRODUCTION

Carbon steel reinforced concrete structures have better compressive, tensile and bending strength than plain concrete structures. But the structure may be destroyed by the corrosion of carbon steel when the passive film on its surface is broken [1, 2]. Among all the destructive factors, chloride

corrosion plays an important role, especially in marine environments [3, 4]. To reduce steel corrosion in a concrete structure, different protection strategies such as cathodic protection, coatings and the addition of corrosion inhibitors have been investigated [5-7]. Among these strategies, adding corrosion inhibitor is the simplest and most effective strategy [8, 9].

Inhibitors retard or prevent the corrosion of carbon steel by influencing the anodic or cathodic process of electrochemical corrosion reactions [10, 11]. Based on the inhibiting mechanism, inhibitors can be divided into three types: anodic-type inhibitors, cathodic-type inhibitors and mixed-type inhibitors. Anodic-type inhibitors such as nitrite, chromate and molybdate can effectively protect passive films of steel, but they may accelerate corrosion when pitting corrosion occurs [12, 13]. Cathodic-type inhibitors include organic compounds such as amines, amides, nitrogen-containing heterocycles and quinoline derivatives, which can absorb on the surface of steel and suppress the cathodic process [14-16]. Though they are eco-friendly, their inhibition performance is not as effective as that of anodic-type inhibitors [17, 18]. Efforts have been made to develop mixed-type inhibitors by synthesizing new chemicals because they contain the advantages of anodic-type and cathodic-type inhibitors. Organic compounds such as 4-(2'-amino-5'-methylphenylazo) antipyrine, 3 fatty acid triazoles, triazole and mercapto-triazole compounds have been proven to be as effective mixed-type inhibitors, that simultaneously act on the anodic and cathodic partial reaction of the corrosion process [19-25].

Although many mixed-type inhibitors have been synthesized and studied, their inhibitory performance and mechanism on carbon steel in concrete environments have not been extensively investigated. In this work, a mixed-type inhibitor named diamino((2-((2-aminoethyl)amino)ethyl)amino)methanethiol (DM) was synthesized. The main aim of this work was to research the effects and mechanism of this newly synthesized inhibitor on retarding corrosion of carbon steel in concrete structures. To rapidly evaluate this inhibition effect and analyse the acting mechanism accurately, electrochemical techniques and surface analysis were carried out in chloride polluted-simulated concrete pore solutions.

## 2. EXPERIMENTAL

### 2.1 Synthesis and characterization of inhibitor

The raw materials diethylenetriamine and thiourea were purchased from Macklin Biochemical Co., Ltd, Shanghai and used without further purification. The studied DM inhibitor was synthesized in our laboratory according to the following steps. Diethylenetriamine (0.1 mol) and thiourea (0.1 mol) were mixed and stirred in a round-bottom flask first, and then heated from room temperature to 80 °C in a 300 mL oil bath under the protection of N<sub>2</sub>. The reaction time was 4 h and the product was stirred until its temperature decreased to the environmental temperature. Then, the product was purified by vacuum distillation to remove the unreacted diethylenetriamine and thiourea, and a brown oily liquid was obtained as the target inhibitor.

The synthesized inhibitor was identified by FT-IR spectroscopy (Nicolet IS10 infrared spectrophotometer, USA) using the KBr pellet method. FT-IR spectrum were obtained in the transmission mode by adding 128 interferograms at  $4\text{ cm}^{-1}$  resolution.

## 2.2 Materials and sample preparation

The carbon steel specimens used in this research are made from Q235 carbon steel with the following chemical composition (wt.%): Mn 0.46, Si 0.26, C 0.17, S 0.017, P 0.0047 and Fe balance. The dimensions of the carbon steel specimens used were  $1.00\text{ cm}\times 1.00\text{ cm}\times 1.00\text{ cm}$  and  $3.00\text{ cm}\times 1.50\text{ cm}\times 1.50\text{ cm}$  for the electrochemical and SEM experiments, respectively. The carbon steel specimens were ground with emery paper (grade 100, 240, 600, 1000 and 2000), degreased in acetone, rinsed with distilled water, and dried at room temperature before the electrochemical experiments. For the electrochemical experiments in the simulated solutions, a cubic carbon steel specimen with a surface exposed to the electrolyte was connected to an electrochemical work station by a copper wire.

The simulated concrete pore solution was prepared with double-distilled water and some analytical grade hydroxide. The concentrations of KOH, NaOH and  $\text{Ca}(\text{OH})_2$  in the simulated solution were 0.60, 0.20 and 0.001 mol/L, respectively. To simulate the corrosion environment of carbon steel, 3.5 wt.% NaCl was added into the simulated concrete pore solution. The obtained solution was used as the corrosion solution. To evaluate the inhibiting effect and analyse the acting mechanism, the DM inhibitor was dissolved in the testing solution at different concentrations, and the solution without DM inhibitor was used as the blank for comparison.

## 2.3 Electrochemical experiments

The electrochemical experiments in this work were performed by a PARSTAT 2273 potentiostat/galvanostat with a classical three-electrode cell system, where the carbon steel specimen acted as the working electrode, a saturated calomel electrode (SCE) was used as the reference electrode and a platinum slice of approximately  $2\text{ cm}^2$  worked as the counter electrode. The three-electrode cell system was immersed in the chloride-polluted simulated concrete pore solution with or without DM for the electrochemical experiments.

Electrochemical impedance spectroscopy measurements were started once the open circuit potential test potential was stable. The excitation signal was a 10 mV peak-to-peak sine wave with current frequency changing from 100 kHz to 10 MHz. The polarization curve measurement was performed after impedance spectroscopy measurement with a scanning rate of  $1\text{ mV s}^{-1}$  from  $-1000\text{ mV}$  to the potential at which the current density increased suddenly. The electrochemical experiments were carried out at  $25 \pm 1\text{ }^\circ\text{C}$  to avoid the influence of the temperature.

## 2.4 Surface observation and analysis

The carbon steel specimens were ground with emery paper (grade 100, 240, 600, 1000 and 2000), degreased with ethyl alcohol and acetone, and dried at room temperature. Then they were

immersed in the chloride-polluted simulated concrete pore solution with and without 1.0% DM inhibitor for 12 h. Then the carbon steel specimens were swashed with distilled water and dried at room temperature. The surface morphology of the specimens was observed using a scanning electron microscope (SEM) (Tabletop Microscope, S3400, HITACHI, Japan), and the elements on the surface of the specimens were obtained using an energy dispersive spectrometer (EDS) X-ray fluorescence (XRF) analysis system (OXFORD Link-ISIS-300, England).

### 3. RESULTS AND DISCUSSION

#### 3.1 Characterization of synthesized inhibitor

Fig. 1 shows the FT-IR transmission spectrum of the synthesized inhibitor. The wide absorption peaks from 3200 to 3400  $\text{cm}^{-1}$  correspond to the N–H bending of  $-\text{NH}_2$  and  $-\text{NH}$ ; the sharp absorption peaks from 1300 to 1500  $\text{cm}^{-1}$  correspond to the C–H bending of  $-\text{CH}_2$  and  $-\text{CH}_3$ ; and the sharp absorption peak near 730  $\text{cm}^{-1}$  corresponds to C–S bending. The absence of an absorption peak near 1100  $\text{cm}^{-1}$  indicates that there is no C=S in the synthesized inhibitor molecule. Considering that no gas was simultaneously produced in the synthetic reaction process, the molecule of the synthesized inhibitor is  $\text{NH}_2(\text{CH}_2)_2\text{NH}(\text{CH}_2)_2\text{NHC}(\text{NH}_2)_2\text{SH}$ .

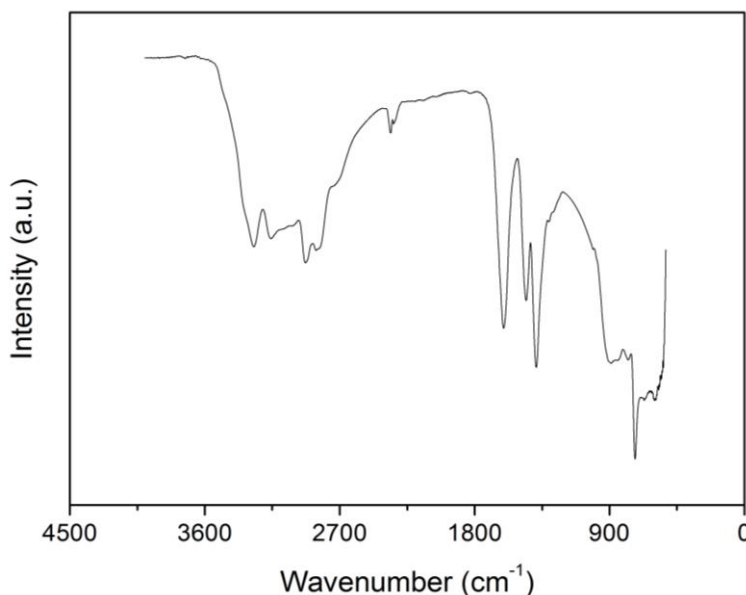


**Figure 1.** Fourier transform infrared transmission spectrum of the synthesized inhibitor

#### 3.2 Electrochemical impedance spectroscopy (EIS)

The received electrochemical impedance plots of the carbon steel specimens immersed in simulated corrosion solutions without and with different DM inhibitor concentrations at 25 °C are shown in Fig. 2. It can be observed from the Nyquist plots that the impedance response changes and the radius of the impedance semicircle increases with the concentration of the DM inhibitor in the

simulated corrosion solution, which indicates that the corrosion resistance of the carbon steel increases with the amount of DM in the corrosion solution [26, 27]. The Bode plots show that the value of the impedance modulus of the corrosion system increases with the concentration of DM inhibitor in the test solution. The phase angle also increases with the concentration of the DM inhibitor, especially in the low-frequency areas. These changes in the Nyquist and Bode plots indicate that the DM inhibitor forms a protective film on the surface of the carbon steel in the test solutions [28, 29].

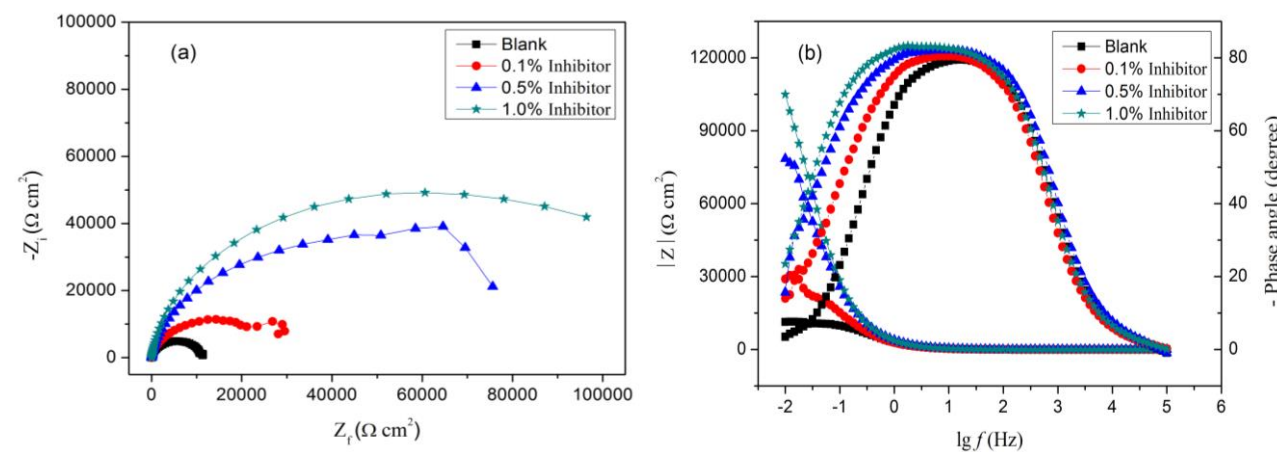


**Figure 2.** Nyquist plots (a) and Bode plots (b) for carbon steel in corrosion solution without and with different concentrations of the DM inhibitor at 25 °C

The electrochemical impedance data obtained from this corrosion system can be analysed and interpreted by the equivalent circuit model illustrated in Fig. 3 [30, 31]. The resistance of the corrosion solution, the resistance of the protective film on the carbon steel surface and the charge transfer resistance of the corrosion process are represented by  $R_s$ ,  $R_f$  and  $R_{ct}$  respectively.  $CPE_1$  is the constant phase angle element that includes the film capacitance ( $C_f$ ) and deviation parameter  $n_1$ , while the constant phase angle element  $CPE_2$  includes the double-layer capacitance ( $C_{dl}$ ) and deviation parameter  $n_2$ .

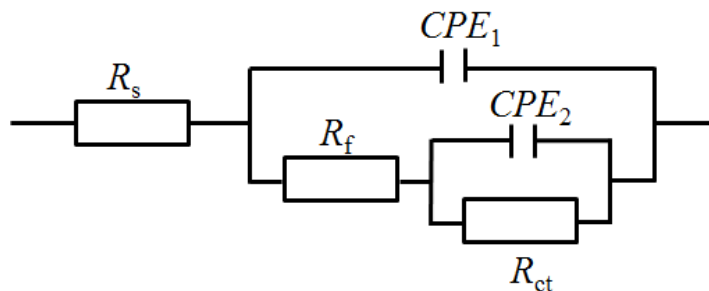


**Figure 3.** Equivalent circuit model used to fit EIS experiment data

The fitted data of the parameters in the equivalent circuit model for carbon steel are listed in Table 1. The value of  $R_f$  increases with the amount of inhibitor in test solution, which reveals that the thickness of the formed protective film on the carbon steel/solution interface increases with the concentration of DM inhibitor [32, 33]. Also, the value of  $R_{ct}$  dramatically increases with the concentration of the DM inhibitor, which indicates that the corrosion process is obviously retarded [34]. According to the electrochemical impedance test results and equivalent circuit model fitted results, the rate of the corrosion reaction is mainly determined by the charge transfer process. Therefore, the EIS measurements can be used to obtain the inhibition efficiency ( $\eta_z$ ) of the inhibitor in the test environment in the following equation [35]:

$$\eta_z = \frac{R_{ct} - R_{ct}^0}{R_{ct}} \times 100\% \quad (3)$$

where  $R_{ct}^0$  and  $R_{ct}$  represent the charge transfer resistance of the corrosion process without and with the DM inhibitor in the corrosion solution, respectively. The value of  $\eta_z$  increases with the concentration of the DM inhibitor, while  $C_{dl}$  decreases with the DM concentration based on the calculated data in Table 1. According to the Helmholtz model,  $C_{dl}$  can be expressed as follows [36]:

$$C_{dl} = \frac{\varepsilon^0 \varepsilon}{d} A \quad (4)$$

where  $\varepsilon^0$  represents the vacuum permittivity,  $\varepsilon$  represents the local dielectric constant,  $d$  represents the thickness of the protective film and  $A$  represents the surface area of the exposed carbon steel electrode. Therefore, the decreased value of  $C_{dl}$  is most likely caused by a decrease in the electrode surface area due to adsorbed inhibitor molecules and the increase in the protective film thickness in this experiment [37-39].

**Table 1.** Electrochemical parameters calculated from the EIS data for carbon steel immersed in corrosion solutions without and with different concentrations of DM inhibitor at 25 °C

Conc. (%)	$R_s$ ( $\Omega \text{ cm}^2$ )	$CPE_1$ ( $\mu\text{F cm}^{-2}$ )	$n_1$	$R_f$ ( $\text{k}\Omega \text{ cm}^2$ )	$CPE_2$ ( $\mu\text{F cm}^{-2}$ )	$n_2$	$R_{ct}$ ( $\text{k}\Omega \text{ cm}^2$ )	$\eta_z$ (%)
0	6.74	58.48	0.91	10.85	1875.0	0.34	1.01	/
0.1	7.31	64.43	0.92	22.96	217.4	0.93	10.01	89.9
0.5	6.51	47.27	0.93	52.96	73.5	0.79	39.03	97.4
1.0	7.49	49.63	0.93	101.30	232.4	0.38	1.48e11	100

### 3.3 Polarization measurements

The polarization curves of the carbon steel specimens in corrosion solutions without and with different DM contents at 25 °C are shown in Fig. 4. The shapes of the anodic and cathodic polarization plots did not change obviously when adding DM inhibitor into the test solution, which suggested that the presence of DM did not change the metal dissolution at the anode and the oxygen reduction reaction at the cathode [40, 41]. The anodic and cathodic polarization curves moved towards current reduction when adding DM inhibitor into the corrosion solution, which indicated that the anodic and cathodic reactions were inhibited and that the corrosion rate was significantly reduced. The inhibitory

effect on the anodic and cathodic reactions increased with the concentration of DM inhibitor in the corrosion solutions. Thus, the inhibition mechanism of DM involves the formation of a protective film on the surface of carbon steel and a reduction in the number of active reactive points [42].

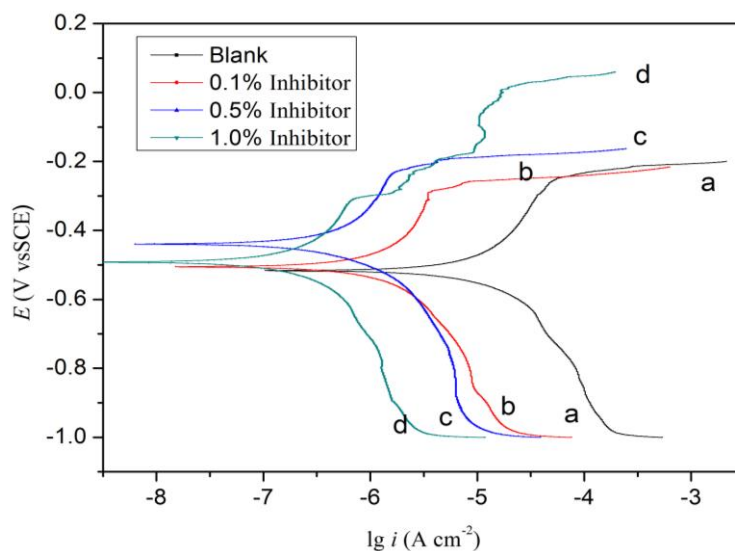


**Figure 4.** Polarization curves of the carbon steel specimens in corrosion solutions without and with different DM contents at 25 °C

The protective film that formed on the carbon steel surface exhibited different characteristics in corrosion solutions with different concentrations of DM inhibitor. For the anodic polarization curve of the carbon steel specimen in a corrosion solution with 0.5% DM inhibitor, the current density increased rapidly when the potential of the working electrode was higher than -220 mV. Under these conditions, the DM molecules desorbed from the electrode surface; thus, this potential was called the desorption potential [43]. The desorption of DM molecules from the electrode surface was caused by obvious carbon steel dissolution, upsetting the adsorption and desorption balance [44]. The anodic polarization curve of the carbon steel specimen in corrosion solution with a 1.0% DM inhibitor, it became unstable and irregular when the electrode potential was between -300 mV and 15 mV. This may be caused by the desorption and reabsorption of DM molecules from the surface of the carbon steel. The desorption of DM molecules was caused by the common function of its own weight and the metal dissolution.

The values of the electrochemical parameters such as the corrosion potential ( $E_{\text{corr}}$ ), corrosion current density ( $i_{\text{corr}}$ ), anodic Tafel slope ( $\beta_a$ ) and cathodic Tafel slope ( $\beta_c$ ) were calculated from the polarization measurements and are listed in Table 2. The  $i_{\text{corr}}$  value decreased as the concentration of DM inhibitor in the corrosion solution increased, which suggested that the corrosion rate of the carbon steel was retarded. The  $E_{\text{corr}}$  value slightly shifted in the positive direction when DM was added into the corrosion solution, and all the changed values of  $E_{\text{corr}}$  were less than 85 mV, which indicated that the inhibitor was a mixed-type corrosion inhibitor [45]. In other words, the DM inhibitor retards the corrosion rate by reducing the reaction surface area of the working electrode without changing the

mechanism of anode or the cathode reaction. The inhibition efficiency ( $\eta_i$ ) can be calculated by the following equation using the obtained polarization measurements [35]:

$$\eta_i = \frac{i_{\text{corr}} - i_{\text{corr}}^0}{i_{\text{corr}}} \times 100\% \tag{5}$$

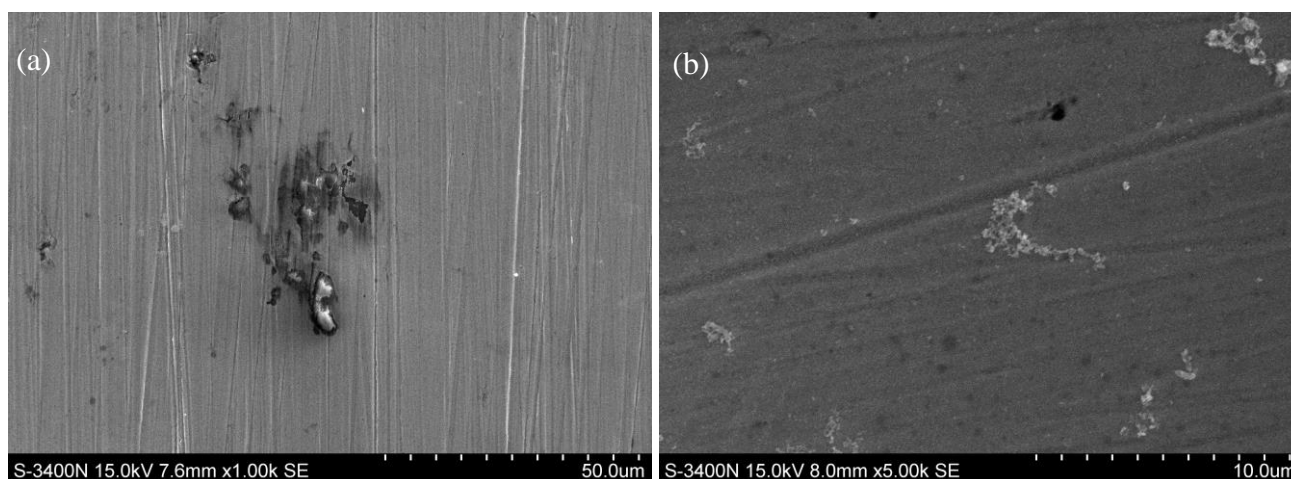
where  $i_{\text{corr}}^0$  and  $i_{\text{corr}}$  present the corrosion current density without and with the DM inhibitor in the corrosion solution, respectively. The table shows that the inhibition efficiency increases with the concentration of DM inhibitor, which agrees with the EIS results.

**Table 2.** Polarization parameters for carbon steel specimen in corrosion solutions without and with different DM contents at 25 °C

Conc. (%)	$E_{\text{corr}}$ (mV)	$\beta_c$ (mV dec <sup>-1</sup> )	$\beta_a$ (mV dec <sup>-1</sup> )	$i_{\text{corr}}$ ( $\mu\text{A cm}^{-2}$ )	$\eta_z$ (%)
0	509	230	288	8.99	/
0.1	501	264	332	1.17	87.0
0.5	435	196	332	0.48	94.7
1.0	496	270	309	0.19	97.9

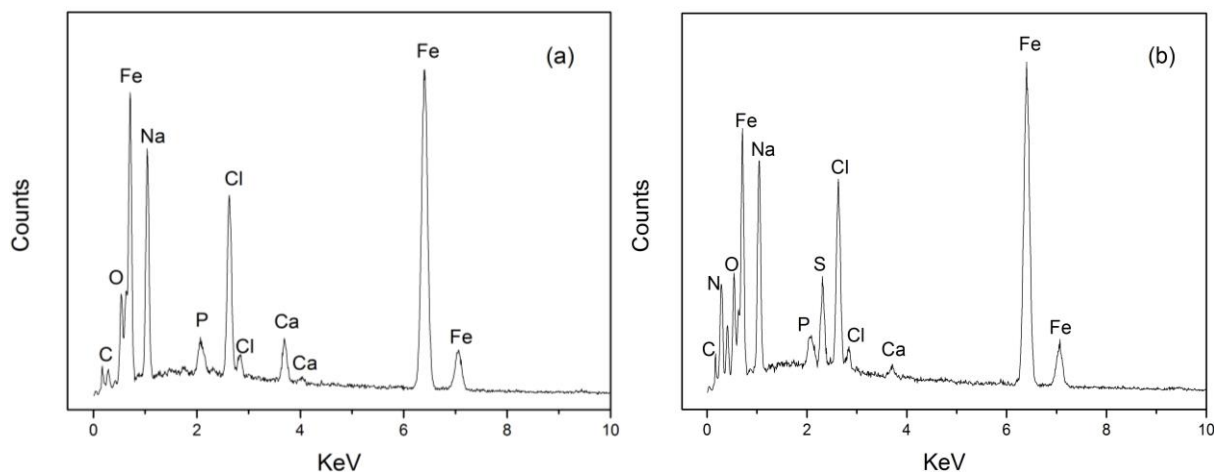
### 3.4. Surface observation and analysis

The SEM images of the carbon steel specimens immersed in the corrosion solution without and with 1.0% DM inhibitor for 12 h are presented in Fig. 5. Compared with the specimen immersed in the simulated solutions with DM inhibitor, the surface of the carbon steel specimen in the absence of inhibitor is relatively rough, and many polishing scratches and local corrosion pits can be observed on the surface. Thus, the carbon steel without the inhibitor was obviously corroded by chloride ions. However, the carbon steel surface is relatively smooth and has few pits in the presence of the DM inhibitors, indicating that the carbon steel specimen is well protected from corrosion.



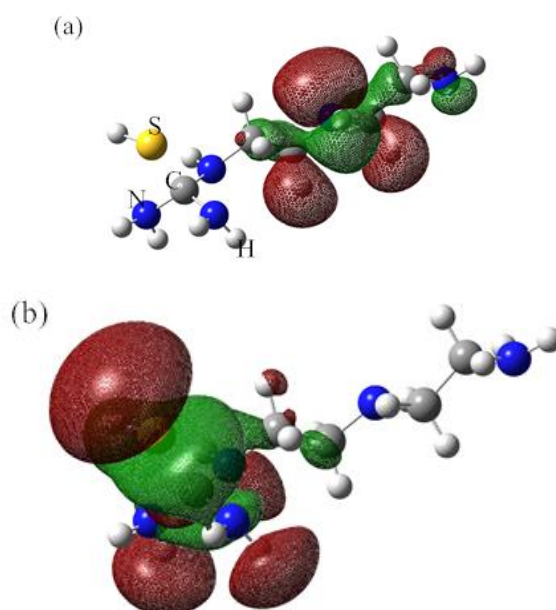
**Figure 5.** SEM morphology of the carbon steel specimens after immersion in corrosion solution without (a) and with (b) 1.0% DM inhibitor for 12 h at 25 °C

Fig. 6 shows the EDS results of the carbon steel specimens immersed in the corrosion solution without and with 1.0% DM inhibitor for 12 h. Compared with the energy diffraction spectrum of the carbon steel specimen immersed without DM inhibitor, the characteristic peaks of N and S elements appeared on the energy diffraction spectrum of the carbon steel specimen with the DM inhibitor. The components of the DM inhibitor revealed that the DM inhibitor can adsorb on the surface of the carbon steel specimen in the corrosion solution. Based on the SEM images and EDS analysis, the DM inhibitor can adsorb on the surface of carbon steel and suppress the corrosion of carbon steel.



**Figure 6.** EDS results for the carbon steel specimens after immersion in corrosion solutions without (a) and with (b) 1.0% DM inhibitor for 12 h at 25 °C

### 3.5. Quantum chemical study



**Figure 7.** The frontier molecular orbital density distribution of the DM molecule: (a) HOMO and (b) LUMO

**Table 3.** Calculated quantum chemical parameters for the DM inhibitor, where  $E_{\text{HOMO}}$  is the energy of the HOMO,  $E_{\text{LUMO}}$  is the energy of the LUMO, and  $\Delta E$  is the energy gap

Name	$E_{\text{HOMO}}$ (eV)	$E_{\text{LUMO}}$ (eV)	$\Delta E$ (eV)	Dipole (debye)
DM inhibitor	-5.76	0.05	5.817	2.68

Quantum chemical calculations with DM molecules were used to explain the adsorption mechanism of DM on the surface of the carbon steel. The electric/orbital density distributions of the highest and lowest occupied molecular orbitals (HOMO & LUMO) for the DM inhibitor are shown in Fig. 7, and the calculated quantum chemical parameters are listed in Table 3.  $E_{\text{HOMO}}$  is associated with the electron donating ability, while  $E_{\text{LUMO}}$  is associated with the electron accepting ability of a molecule [46, 47]. Lower absolute value of  $E_{\text{HOMO}}$  and  $E_{\text{LUMO}}$  indicate stronger electron donating and accepting abilities, respectively, of a molecule, and the higher value of  $\Delta E$  indicates the higher stability of a molecule [48]. The very low energy value of the LUMO, indicates that the DM inhibitor molecule can adsorb on the surface of carbon steel based on acceptor–donor interactions between the unstable electrons in the semi-full d-orbitals of the iron atoms and the –C–N–H and –C–S–H groups of the DM molecule.

#### 4. CONCLUSIONS

In this research, the inhibition performance of a synthesized DM inhibitor on the corrosion of carbon steel in a chloride-polluted simulated concrete pore solution was studied systematically. The carbon steel electrochemical experiments in the simulated solution allowed a rapid evaluation of the inhibition performance of the synthesized DM inhibitor, and the electrochemical analysis, carbon steel surface analysis from SEM and EDS and quantum chemical calculations revealed the inhibition mechanism of the DM inhibitor. From the obtained results, the following conclusions can be drawn:

1. The synthesized DM inhibitor showed a good inhibition effect for the carbon steel immersed in a chloride-polluted simulated concrete pore solution. The inhibition effect gradually increased as the concentration of the DM inhibitor increased from 0 to 1.0% in this work.
2. The DM molecules can adsorb on the surface of the carbon steel specimen and form a protective film in the corrosion solution, which can suppress both the anodic and cathodic processes of the carbon steel corrosion reaction by reducing the number of active reactive points.
3. The adsorption of DM inhibitor molecules on the surface of carbon steel specimens is based on acceptor–donor interactions between the unstable electrons of the semi-full d-orbitals of iron atoms and the –C–N–H and the –C–S–H groups of the DM molecules.
4. The DM inhibitor performed as a mixed-typed inhibitor in effectively inhibiting the corrosion process of carbon steel in an alkaline environment, which indicates its potential to be used as a carbon steel inhibitor in real concrete structures.

This work shows that the DM inhibitor has the capacity to retard the corrosion of carbon steel in an alkaline environment. However, our work was limited to evaluating the performance of the DM inhibitor in a simulated medium rather than in an actual application environment. For example, we used a simulated pore solution to simulate the actual concrete environment without considering ions such as  $\text{SO}_4^{2-}$  and  $\text{CO}_3^{2-}$ , and we used a 3.5% NaCl solution to simulate seawater corrosion medium without considering other positive or negative ions. In addition, the corrosion process of carbon steel in a concrete structure is a slow, long and complex process influenced by many parameters such as the external environment and properties of concrete. Considering all these factors, a long process of static coupon testing of reinforced concrete in an actual marine environment may be the most objective and effective method to assess the inhibiting effect of DM.

#### ACKNOWLEDGEMENTS

The authors would like to gratefully acknowledge the support of the National Key Projects of China (2016YFC0700800), the National Science Foundation of China (NO. 21466023), the Postdoctoral Fund of China (2016M592256), the Shandong Provincial Key Research and Development Plan (NO. 2017GHY15118) and the Nantong Science and Technology Plan (NO. GY12016046).

#### References

1. M. Ormellese, M. Berra, F. Bolzoni, T. Pastore, *Cem. Concr. Res.*, 36 (2006) 536.
2. L. Jiang, G. Huang, J. Xu, Y. Zhu, L. Mo, *Constr. Build. Mater.*, 30 (2012) 516.
3. K. Y. Ann, H. Song, *Corros. Sci.*, 49 (2007) 4113.
4. Y. Hui, K. K. Chiang, L. Yang, *Constr. Build. Mater.*, 26 (2012) 723–729.
5. D.Z. Tang, Y. X. Du, M. X. Lu, Z. T. Jiang, L. Dong, J. J. Wang, *Mater. Corros.*, 66 (2015) 278.
6. R. Ramanauskas, O. Girčienė, L. Gudavičiūtė, A. Selskis, *Appl. Surf. Sci.*, 327 (2015) 131.
7. H. Zheng, W. Li, F. Ma, Q. Kong, *Constr. Build. Mater.*, 37 (2012) 36.
8. K.F. Khaled, *Electrochim. Acta*, 54 (2009) 4345.
9. A. Zarrouk, B. Hammouti, R. Touzani, R. Elkadiri, *Int. J. Electrochem. Sci.*, 6 (2011) 4939.
10. I.A. Kartsonakisa, S.G. Stanciub, A.A. Mateib, E.K. Karaxia, R. Hristub, A. Karantonisa, C.A. Charitidisa, *Corros. Sci.*, 100 (2015) 194.
11. S. Bohm, H.N. McMurray, D.A. Worsley, S.M. Powell, *Mater. Corros.*, 52 (2001) 896.
12. S.S. Abd El Rehim, H.H. Hassan and N.F. Mohamed, *Corros. Sci.*, 46 (2004) 1071.
13. A. Poursaee, C.M. Hansson, *Cem. Concr. Res.*, 39 (2009) 391.
14. Zarrouk, B. Hammouti, H. Zarrok, M. Bouachrine, K.F. Khaled, S.S. Al-Deyab, *Int. J. Electrochem. Sci.*, 7 (2012) 89.
15. Z. Yang, H. Fischer, J. Cerezo, J.M.C. Mol, R. Polder, *Mater. Corros.*, 67 (2016) 721.
16. N. Nakayam, A. Obuchi, *Corros. Sci.*, 45 (2003) 2075.
17. H. Zheng, W. Li, F. Ma, Q. Kong, *Cem. Concr. Res.*, 55 (2014) 102.
18. X. Zhao, C. Kun, W. Li, Z. Jin, B. Hou, *Int. J. Electrochem. Sci.*, 8(2013) 7948.
19. Y. Yan, W. Li, L. Cai, B. Hou, *Electrochim. Acta*, 53 (2008) 5953.
20. F.M. AlKharafi, N.A. Al-Awadi, I.M. Ghayad, R.M. Abdullah, M.R. Ibrahim, *Int. J. Electrochem. Sci.*, 6 (2011) 1562.
21. W. Li, L. Hu, S. Zhang, B. Hou, *Corros. Sci.*, 53 (2011) 735.
22. M.A. Quraishi, D. Jamal, *Mater. Chem. Phys.*, 68 (2001) 283.
23. S.S. Abd El Rehim, M.A.M. Ibrahim, K.F. Khalid, *Mater. Chem. Phys.*, 70 (2001) 268.
24. H.L. Wang, R.B. Liu, J. Xin, *Corros. Sci.*, 46 (2004) 2455.

25. G. Zhang, C. Chen, M. Lu, C. Chai, Y. Wu, *Mater. Chem. Phys.*, 105 (2007) 331.
26. X. Zhao, K. Cao, W.H. Li, Z.Q. Jin, B.R. Hou, *Int. J. Electrochem. Sci.*, 8 (2013) 8513.
27. K. Cao, W.H. Li, L.M. Yu, *Int. J. Electrochem. Sci.*, 7 (2012) 806.
28. X. Zhou, H. Yang, F. Wang, *Electrochim. Acta*, 56 (2011) 4268.
29. H.E. Jamil, M.F. Montemor, R. Boulif, A. Shrir, M.G.S. Ferreira, *Electrochim. Acta*, 48 (2003) 3509.
30. Q.A. Huang, R. Hui, B. Wang, J. Zhang, *Electrochim. Acta*, 52 (2007) 8144.
31. Z. Tao, S. Zhang, W. Li, B. Hou, *Corros. Sci.*, 51 (2009) 2588.
32. K.A. Alawi Al-Sodani, O. S. Baghabra Al-Amoudi, M. Maslehuddin, M. Shameem, *Constr. Build. Mater.*, 163 (2018) 97.
33. Y. Qiang, S. Zhang, S. Yan, X. Zou, S. Chen, *Corros. Sci.*, 126 (2017) 295.
34. F.E. Heikal, A.E. Elkholy, *J. Mol. Liq.*, 230 (2017) 395.
35. K. F. Khaled, *Electrochim. Acta*, 54 (2009) 4345.
36. K. Cao, Q. Wang, T. Tian, *Int. J. Electrochem. Sci.*, 12 (2017) 7537.
37. T. Hu, H. Shi, T. Wei, F. Liu, S. Fan, E.H. Han, *Corros. Sci.*, 95 (2015) 152.
38. M. Cui, S. Ren, Q. Xue, H. Zhao, L. Wang, *J. Alloy Compd.*, 726 (2017) 680.
39. A. Biswas, S. Pal, G. Udayabhanu, *Appl. Surf. Sci.*, 353 (2015) 173.
40. Z.Z. Tasic, M.B. Petrovic Mihajlovic, M.B. Radovanovic, A.T. Simonovic, M.M. Antonijevic, *J. Mol. Struct.*, 1159 (2017) 46.
41. E.B. Ituen, O. Akaranta, S.A. Umoren, *J. Mol. Liq.*, 246 (2017) 112.
42. M. Goyal, S. Kumar, I. Bahadur, C. Verma, E.E. Ebenso, *J. Mol. Liq.*, 256 (2018) 565.
43. W.J. Lorenz, F. Mansfeld, *Corros. Sci.*, 21 (1981) 647.
44. A.A. Aksut, W.J. Lorenz, F. Mansfeld, *Corros. Sci.*, 22 (1982) 611.
45. H. Ashassi-Sorkhabi, M.R. Majidi, K. Seyyedi, *Appl. Surf. Sci.*, 225 (2004) 176.
46. H. Hamani, T. Douadi, M. Al-Noaimi, S. Issaadi, D. Daoud, S. Chafaa, *Corros. Sci.*, 88 (2014) 234.
47. L.C. Murulana, M.M. Kabanda, E.E. Ebenso, *J. Mol. Liq.*, 215 (2016) 763.
48. N. Khalil, *Electrochim. Acta*, 48 (2003) 2635.

© 2018 The Authors. Published by ESG ([www.electrochemsci.org](http://www.electrochemsci.org)). This article is an open access article distributed under the terms and conditions of the Creative Commons Attribution license (<http://creativecommons.org/licenses/by/4.0/>).